International Journal of Engineering Research and Science & Technology

www.ijerst.org

ISSN : 2319-5991

Vol. 22 No. 1(s) (2026)



ijerst.editor@gmail.com

editor@ijerst.com

www.ijerst.com
© 2026 IJERST. All Rights Reserved
Peer Reviewed, Referred & Indexed Journal

Research Paper

Investigation of the structural and optical properties of g-C_3N_4 Microstructure and their photocatalytic performance for MB dye degradation.

Dnyaneshwar Misal[a], Dhirsing Naik[a], Pravin Ghare[b], Madhukar Navgire[a*]

[a]Department of Chemistry, Jijamata College of Science and Arts, Bhende, 414605, MS, India

[b]Department of Physics, Jijamata College of Science and Arts, Bhende, 414605, MS, India

Email: dnyaneshwarmisal50@gmail.com

Abstract

Graphitic carbon nitride (g-C_3N_4) was synthesized via a simple calcination method from thiourea precursors, and its structural, optical, and photocatalytic properties were investigated. FTIR spectroscopy indicated the presence of triazine rings and nitrogen-containing functional groups. T-GCN and Ultrasonication T-GCN exhibited superior photocatalytic activity, achieving 22.22% and 38.64% MB degradation, respectively. After ultrasonication, T-GCN showed improved light absorption and charge-carrier transport.

Introduction

Semiconductor-based photocatalysis has emerged as a promising and sustainable strategy for degrading organic pollutants in wastewater, particularly textile dyes, pharmaceutical residues, and industrial effluents. Traditional treatment methods often suffer from incomplete mineralization and secondary contamination, thereby necessitating the development of efficient visible-light-driven photocatalysts. Among various semiconductor materials, polymeric graphitic carbon nitride (g-C_3N_4) has attracted significant attention due to its metal-free composition, suitable band gap (~2.7 eV), high physicochemical stability, low cost, and visible-light responsiveness [1–3].

g-C_3N_4 consists of tri-s-triazine (heptazine) units linked through planar amino bridges, forming a two-dimensional layered structure analogous to graphite but enriched with nitrogen atoms. This nitrogen-rich conjugated framework enables strong π–π electron delocalization, which governs its semiconducting and photocatalytic properties [2,4]. The valence band (VB) of g-C_3N_4 is mainly derived from N 2p orbitals, whereas the conduction band (CB) is composed predominantly of C 2p orbitals, facilitating visible-light absorption and photogenerated charge carrier formation under solar irradiation [3,5]. Upon visible-light

excitation, electrons are promoted from the VB to the CB, generating electron–hole (e^-/h^+) pairs. These charge carriers migrate to the surface and participate in redox reactions, forming reactive oxygen species (ROS) such as superoxide radicals ($\bullet O_2^-$) and hydroxyl radicals (•OH), which are responsible for the degradation and mineralization of organic pollutants [3,6]. However, rapid charge-carrier recombination, limited surface area, and moderate conductivity often limit the intrinsic photocatalytic performance of bulk g-C_3N_4 [5–7].

Therefore, tailoring the structural and optical properties of g-C_3N_4 microstructures is essential to enhance photocatalytic efficiency. Structural parameters such as crystallinity, interlayer stacking, defect density, nitrogen configuration, and surface morphology significantly influence charge separation and active site availability [4,7]. Similarly, optical properties, including band gap energy, light absorption range, and photoluminescence behavior, determine the efficiency of photon harvesting and the dynamics of electron–hole recombination [3,6]. Recent studies have demonstrated that microstructural engineering strategies such as exfoliation, heterojunction formation, elemental doping, and defect modulation can effectively enhance visible-light absorption and suppress recombination losses **[6–9]**. Consequently, understanding the correlation between structural characteristics and optical behavior is crucial for optimizing photocatalytic degradation performance.

In this context, the present work systematically investigates the structural and optical properties of g-C_3N_4 microstructures and correlates them with photocatalytic degradation efficiency. Comprehensive characterization technique, including X-ray diffraction (XRD), Fourier transform infrared spectroscopy (FTIR), Raman spectroscopy, and UV-Vis diffuse reflectance spectroscopy (UV-DRS). Further, preserving the intrinsic bonding environment is crucial for maintaining the electronic structure and, consequently, the photocatalytic performance.

2. Experimental methodology

2.1 Chemicals

The precursors used to synthesize g-C_3N_4 were thiourea (CH_4N_2S, 99%, Sigma-Aldrich). No additional purification was required, as all chemicals were of analytical grade.

Synthesis of g-C_3N_4

To synthesize T-GCN, 10 g of thiourea was ground in a mortar and pestle. The resulting white powder was transferred to a crucible with a lid and then calcined at 550 °C for 3 h at a controlled heating rate of 5 °C/min. After calcination, the sample was allowed to cool naturally to ambient conditions. The final yellowish product was ground in an agate mortar to obtain a fine yellow powder. The schematic shows the synthesis of g-C_3N_4 using thiourea.

Furthermore, 2 M HCl and 50 mL DDW were combined and ultrasonicated continuously for up to 3 h to obtain g-C_3N_4 from thiourea.

3 Results and Discussion

3.1 RAMAN analysis

The Raman spectrum of g-C_3N_4 reveals characteristic vibrational features confirming the formation of a nitrogen-rich polymeric network composed of tri-s-triazine (heptazine) units. A prominent peak observed at ~700–710 cm^{-1} is assigned to the breathing mode of the heptazine ring. This vibrational mode is widely recognized as a fingerprint of polymeric graphitic carbon nitride and confirms successful condensation of nitrogen-containing precursors into a layered conjugated framework [10,11]. In the intermediate spectral region (1200-1400 cm^{-1}), several bands originate from C-N heterocyclic vibrations. The peak at ~1230-1250 cm^{-1} corresponds to stretching vibrations of sp^2-hybridized C-N bonds involving bridging nitrogen atoms, whereas the band near ~1310-1350 cm^{-1} is attributed to aromatic C-N stretching within the heterocyclic framework [11,12]. These features indicate the presence of a highly conjugated C-N network, dominated by nitrogen atoms, which is responsible for the electronic delocalization and semiconducting behavior of g-C_3N_4. In the high wavenumber region (1500-1650 cm^{-1}), a broad band centered at ~1560-1580 cm^{-1} is assigned to C=N stretching vibrations within the aromatic heptazine units. This band partially overlaps with the graphitic G-band and reflects the conjugated π-electron system involving both carbon and nitrogen atoms [12,13]. The strong contribution of nitrogen-containing vibrational modes underscores the nitrogen-rich composition of g-C_3N_4, in which tertiary nitrogen $(N\text{-}C)_3$ and pyridinic nitrogen species modulate its electronic structure.

Additionally, a band near ~1350 cm^{-1} can be associated with the D-band, which arises from structural disorder, nitrogen vacancies, or edge defects within the layered structure. The band around ~1580 cm^{-1} corresponds to the G-band (E_2g mode) of sp^2-bonded carbon atoms. The relative intensity ratio (I_D/I_G) provides insight into the defect density and degree of graphitization [13]. In nitrogen-rich g-C_3N_4, defect formation is often associated with nitrogen vacancies or incomplete polymerization, thereby significantly influencing photocatalytic and charge-transport properties. Overall, the Raman spectral characteristics confirm the formation of polymeric g-C_3N_4 with a conjugated heptazine-based architecture. The dominance of C–N and C=N vibrational modes reflects the nitrogen-rich heterocyclic framework that governs its electronic structure and functional performance [10–13].

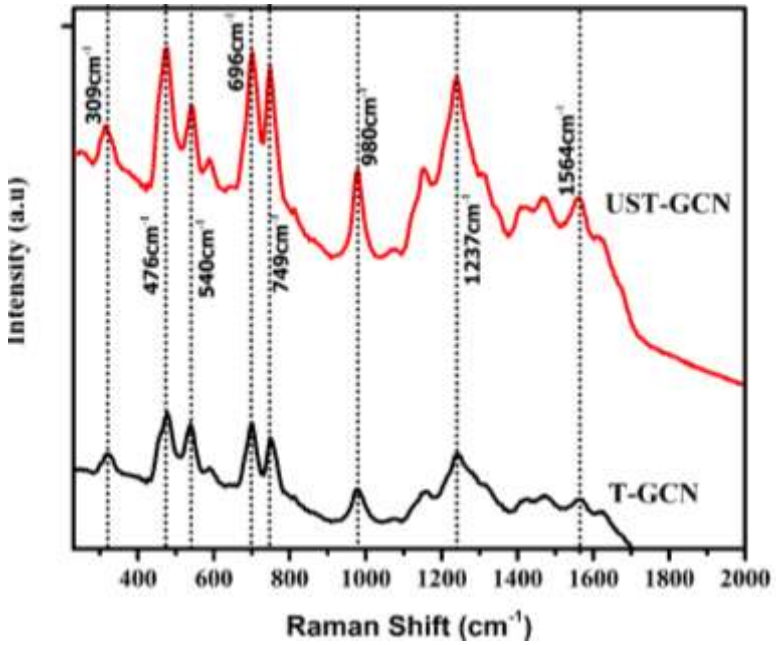


Figure 1. Raman spectra of T-GCN, (d) ultra-sonication of T-GCN

3.2 Fourier Transform Infrared Spectroscopy (FT-IR)

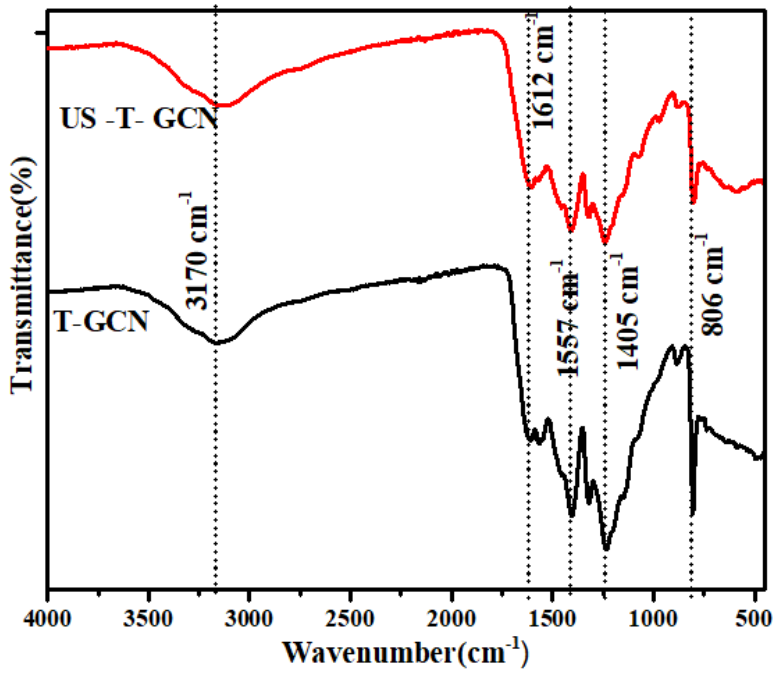


Figure 2. FTIR spectra of (a) T-GCN, (b) ultra-sonication of T-GCN.

The FTIR spectrum reveals distinct absorption bands corresponding to N–H, C=C, C–H, C–N, and C–O functional groups, confirming the presence of heteroatomic and aromatic structural units in the material. The vibrational frequencies, force constants, and calculated bond lengths provide insight into bond strength and molecular stability [14]. The high-frequency band observed at 3170 cm^{-1} is assigned to N–H stretching vibration. The relatively large force constant (4.97×10^4 dynes·cm^{-1}) indicates significant bond stiffness, suggesting

strong intermolecular interactions or hydrogen bonding effects. The calculated bond length (~1.020 Å) is consistent with typical N–H bond distances, confirming structural integrity. The FTIR spectra of T-GCN and ultra-sonicated T-GCN, as shown in Fig. 2, are nearly identical, with no additional absorption bands or noticeable peak shifts observed after 3 hours of continuous ultrasonication [15]. This clearly indicates that ultrasonication does not induce any new chemical bonds or structural transformations in the polymeric framework of graphitic carbon nitride. All characteristic vibrational features associated with the heptazine (tri-s-triazine) units, including the stretching modes of C-N and C=N bonds in the 1200-1650 cm^{-1} region, remain unchanged. Hence, ultrasonication primarily affects physical or morphological properties, such as exfoliation or dispersion, without disrupting the intrinsic covalent network. To gain quantitative insight into the bonding characteristics, force constants and bond lengths were evaluated from the FTIR vibrational frequencies. The force constant (k) for each mode was calculated using the harmonic oscillator approximation [16]**:**

$$v = \frac{1}{2\pi c}\sqrt{\frac{k}{\mu}}$$

Where $\mu = \frac{m_1.m_2}{m_1+m_2}$ is the reduced mass of the bonded atoms. Rearranging the above expression gives:

$$k = v^2 4\pi^2 c^2 \mu$$

The calculated force constants were subsequently used to estimate bond lengths employing the modified Badger's rule proposed by Richard M. Badger:

$$R = \sqrt[3]{\frac{C_{ij}}{k}} + d_{ij}$$

where C_{ij} and d_{ij} are empirical fitting constants dependent on the nature and periodic position of the bonded atoms. For g-C_3N_4, the values C_{ij} = 0.535 Å and d_{ij} = 0.94 Å were used. The calculated results show that the N–H stretching vibration at 3170 cm^{-1} possesses a relatively high force constant, indicating strong bond stiffness [17]. The C=C stretching mode around 1605 cm^{-1} exhibits the highest force constant among all observed vibrations, confirming the strong double-bond character and extended conjugation within the g-C_3N_4 framework. The C-N stretching bands appearing at 1323 and 1240 cm^{-1} display moderate force constants, consistent with stable sp^2-hybridized C-N linkages in the heptazine units. In contrast, the C-H bending and out-of-plane deformation modes observed at lower wavenumbers show significantly smaller force constants, as expected for bending vibrations

[18]. The difference in force constants or calculated bond lengths is observed between T-GCN and ultra-sonicated T-GCN samples. The bond lengths obtained from Badger's rule remain within the expected range for conjugated C-N systems, confirming that prolonged ultrasonication does not disrupt the covalent skeleton of g-C_3N_4. Overall, the combined FTIR spectral analysis and bond length calculations demonstrate the excellent structural robustness and chemical stability of g-C_3N_4 under ultrasonication. Preserving the intrinsic bonding environment is crucial for maintaining the electronic structure and, consequently, the photocatalytic performance [19].

Table 1 The calculation of T-GCN force constant and bond length (Å)

Sr. No	Function group	Wavenumber (cm^{-1})	Force Constant ($dynes.cm^{-1}$)	Bond Length (Å)
1	N-H	3170	4.97×10^4	1.020
2	C=C	1612	8.19×10^4	0.952
3	C=C	1557	7.71×10^4	0.953
4	O-H	1405	9.85×10^3	0.965
5	C-N	1316	5.92×10^4	0.954
6	C-O	1233	5.50×10^4	0.954
7	C-H	886	3.84×10^3	0.974
8	C-H	806	3.18×10^3	0.976

Table 2: The calculation of the Ultra-Sonication of T-GCN force constant and bond length (Å)

Sr. No	Function group	Wavenumber (cm^{-1})	Force Constant ($dynes.cm^{-1}$)	Bond Length (Å)
1	N-H	3170	4.97×10^4	1.020
2	C=C	1605	8.26×10^4	0.952
3	C-H	1405	9.67×10^3	0.965
4	C-N	1323	9.85×10^3	0.965
5	C-N	1240	5.27×10^4	0.954
6	C-O	1068	4.14×10^4	0.956
7	C-H	882	3.81×10^3	0.974
8	C-H	799	3.12×10^3	0.977

4. Application of synthesized of g-C_3N_4 and UST-g-C_3N_4 materials

4.1 Photocatalytic dye degradation

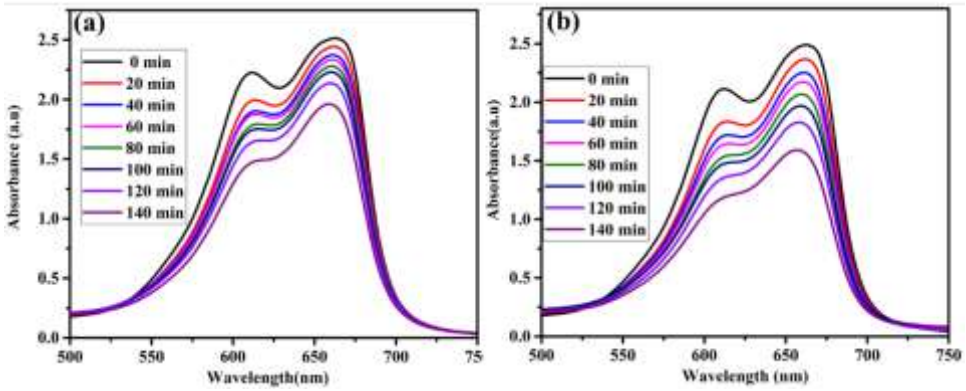


Fig. 3. UV-visible absorption spectra for the MB dye with catalyst (a)T-GCN and (b) Ultra-Sonication of T-GCN

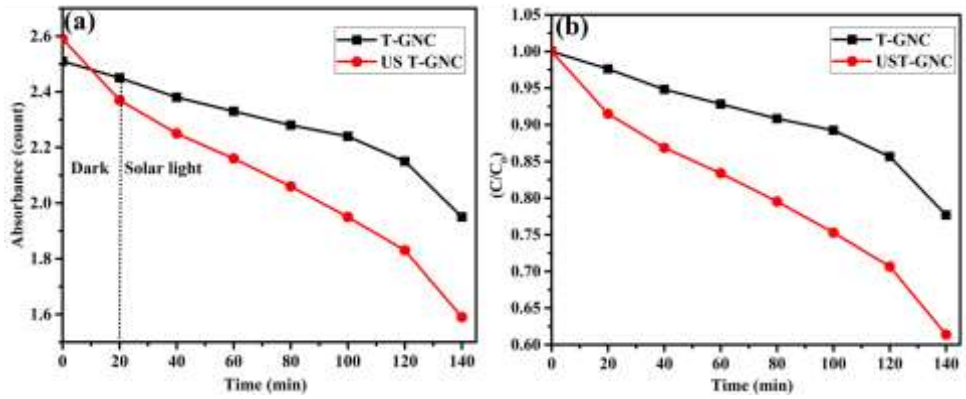


Fig. 4. Absorbance count and its photodegradation of the MB dye with catalyst (a)T-GCN and (b)Ultra-Sonication of T-GCN

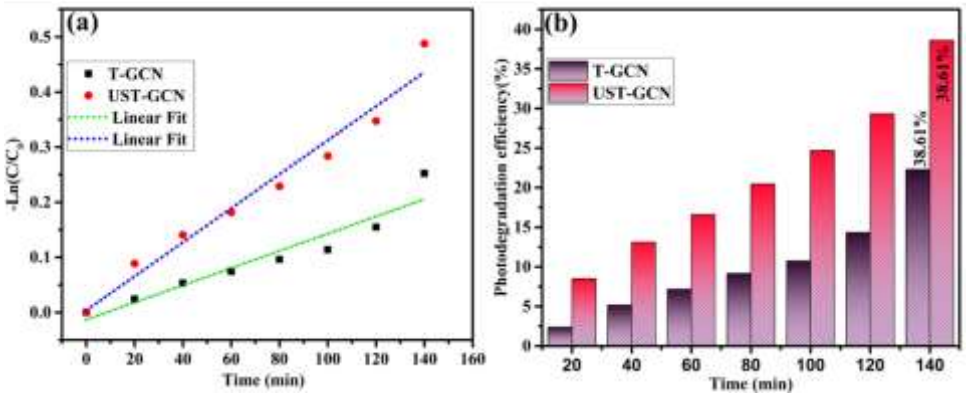


Fig. 5. (a) Linear Fit of the pseudo-first-order kinetic reaction and (b) Photodegradation efficiency of the T-GCN and Ultra-Sonication of T-GCN

Fig. 1 shows the UV–Visible absorption spectra of Methylene Blue (MB) under solar irradiation (0–140 min) in the presence of thermally prepared g-C_3N_4 (T-GCN) and ultrasonicated g-C_3N_4 (UST-GCN). MB exhibits a characteristic absorption peak at approximately 664 nm, corresponding to its chromophoric thiazine structure [20]. A gradual decrease in peak intensity with increasing irradiation time confirms the photocatalytic

degradation of MB. Notably, no significant shift in λ_{max} is observed, indicating that degradation occurs through mineralization rather than structural transformation of the chromophore [21]. For T-GCN (without sonication), the absorbance at 664 nm decreases steadily from 0 to 140 min, demonstrating moderate photocatalytic activity. In contrast, UST-GCN shows a much faster reduction in peak intensity, indicating enhanced degradation efficiency. The photocatalytic experiment consists of two stages: (i) first, dark adsorption (0-20 min) and (ii) solar irradiation (20-140 min). During the dark phase, a slight decrease in absorbance is observed for both catalysts, due to adsorption of MB molecules onto their surfaces. UST-GCN exhibits a higher adsorption capacity, which can be attributed to reduced particle size, increased surface area, improved dispersion, and greater exposure of active sites under solar irradiation. Both catalysts show continuous degradation of MB, but UST-GCN exhibits a significantly faster decline in absorbance than T-GCN. After 140 min, the absorbance of UST-GCN is markedly lower, confirming its superior photocatalytic performance. Furthermore, the photodegradation efficiency is calculated using the following equation.

$$\text{Degradation (\%)} = \left(1 - \frac{C}{C_0}\right) \times 100$$

Where C_0 is the initial concentration, and C is the concentration over time t =140 min of irradiation: T-GCN, the degradation efficiency achieved for 22.22%, and UST-GCN, for 38.67%. Although the final numerical values appear close, the time-dependent degradation profile clearly indicates that UST-GCN maintains consistently higher degradation efficiency throughout the irradiation period. The improved performance of UST-GCN is attributed to structural modifications induced by ultrasonication, which enhance photocatalytic properties [22]. The figure shows the pseudo-first order kinetic reactions plot of axis along the -ln (C/C_0) vs Over time (t), which is applied linear fitting equation, and calculated by the following equation

$$ln\left(\frac{C_0}{C}\right) = -kt$$

Where k is the apparent rate constant (min^{-1}). The linear relationship between $-\ln(C/C_0)$ and irradiation time confirms pseudo-first-order kinetics for both catalysts. The slope of the fitted line corresponds to the rate constant k. as shown in the table

Table 3 Photocatalytic activity performance

Sr. No	Name	Rate constant	Efficiency	Linear Fit (R^2)
1	T-GCN	0.00359	22.22	0.9875

2	UST-GCN	0.00711	39.61	0.09617

UST-GCN exhibits a steeper slope compared to T-GCN, indicating: Higher apparent rate constant, Faster reaction kinetics, Improved charge carrier utilization. This enhancement is primarily due to reduced electron–hole recombination and improved interfacial charge transfer [23].

Photocatalytic Dye Degradation Mechanism

In pristine T-GCN and UST-GCN, absorption of photons with energy ≥2.7 eV promotes electrons from the valence band (VB) to the conduction band (CB), leaving behind holes (h^+). However, UST-GCN and T-GCN suffer from fast recombination of photogenerated carriers, which significantly limits the production of reactive oxygen species (ROS) such as superoxide radicals ($^{\bullet}O_2^-$) and hydroxyl radicals (•OH). Under solar irradiation, g-C_3N_4 absorbs visible light due to its band gap (~2.7 eV).

g-C_3N_4 + $h\nu$ or T-GCN Or SUT-GCN$\rightarrow\left(e^-_{(CB)}\right)+\left(h^+_{(VB)}\right)$($E_{Photon}$ – charge carrier created) The generated charge carriers participate in redox reactions:

$$\left(h^+_{(VB)}\right)+H_2O\rightarrow\textbf{(•OH)}$$

$$\left(e^-_{(CB)}\right)+O_2\rightarrow\textbf{(•}\boldsymbol{O_2^-}\textbf{)}$$

The reactive oxygen species **(•OH)** and **(•$\boldsymbol{O_2^-}$)** oxidize MB molecules into intermediate products, eventually mineralizing them into CO_2 and H_2O. Ultrasonication enhances this mechanism by increasing the number of surface-active sites, improving light absorption, facilitating charge separation, and suppressing electron–hole recombination. As a result, UST-GCN shows superior solar-driven photocatalytic performance compared to T-GCN [24]

Conclusion

In summary, graphitic carbon nitride was successfully synthesized from thiourea precursors, yielding unique properties that enhance its photocatalytic activity under visible light. The results showed that US-T-GCN exhibited higher MB degradation efficiency (38.61%) than T-GCN without sonication (22.22%). This study highlights that the choice of ultrasonication material influences the properties of g-C_3N_4 , demonstrating that the improved structural and optical properties of US-T-GCN make it a potential candidate for environmental applications.

Reference

1. Wang X, Maeda K, Thomas A, et al. A metal-free polymeric photocatalyst for hydrogen production from water under visible light. *Nature Materials*. 2009; 8:76–80. https://doi.org/10.1038/nmat2317.
2. Thomas A, Fischer A, Goettmann F, et al. Graphitic carbon nitride materials: variation of structure and morphology and their use as metal-free catalysts. *Journal of Materials Chemistry*. 2008; 18:4893–4908. https://doi.org/10.1039/B800274F
3. Ong WJ, Tan LL, Ng YH, Yong ST, Chai SP. Graphitic carbon nitride ($g-C_3N_4$)-based photocatalysts for artificial photosynthesis and environmental remediation. *Chemical Reviews*. 2016; 116:7159–7329. https://doi.org/10.1021/acs.chemrev.6b00075
4. Algara-Siller G, Severin N, Chong SY, et al. Triazine-based graphitic carbon nitride: a two-dimensional semiconductor. *Angewandte Chemie International Edition*. 2014; 53:7450–7455. https://doi.org/10.1002/anie.201402846
5. Niu P, Zhang L, Liu G, Cheng HM. Graphene-like carbon nitride nanosheets for improved photocatalytic activities. *Advanced Functional Materials*. 2012; 22:4763–4770. https://doi.org/10.1002/adfm.201200922
6. Dong F, Zhao Z, Xiong T, et al. In situ construction of $g-C_3N_4$-based heterojunction for enhanced visible-light photocatalysis. *ACS Applied Materials & Interfaces*. 2013;5:11392–11401. https://doi.org/10.1021/am402629p
7. Zhang J, Chen Y, Wang X. Two-dimensional covalent carbon nitride nanosheets: synthesis, functionalization, and applications. *Energy & Environmental Science*. 2015; 8:3092–3108. https://doi.org/10.1039/C5EE01895A
8. Kumar S, et al. Defect-engineered graphitic carbon nitride for enhanced photocatalysis. *Applied Catalysis B: Environmental*.2017;205:629639 .https://doi.org/10.1016/j.apcatb.2016.12.056
9. Cao S, Yu J. $g-C_3N_4$-based photocatalysts for hydrogen generation. *Journal of Physical Chemistry Letters*.2014;5:2101–2107. https://doi.org/10.1021/jz500546b
10. Wang X, Maeda K, Thomas A, et al. A metal-free polymeric photocatalyst for hydrogen production from water under visible light. *Nature Materials*.2009;8:76–80. https://doi.org/10.1038/nmat2317.
11. Thomas A, Fischer A, Goettmann F, et al. Graphitic carbon nitride materials: variation of structure and morphology and their use as metal-free catalysts. *Journal of Materials Chemistry*. 2008;18:4893–4908. https://doi.org/10.1039/B800274F.
12. Zhang J, Zhang M, Sun RQ, Wang X. A facile band alignment of polymeric carbon nitride semiconductors to construct isotype heterojunctions. *Angewandte Chemie International Edition*.2012;51:10145–10149. https://doi.org/10.1002/anie.201204053.
13. Ferrari AC, Robertson J. Interpretation of Raman spectra of disordered and amorphous carbon.*PhysicalReviewB*.2000;61:1409514107 .https://doi.org/10.1103/PhysRevB.61.14095.
14. Wang X, Maeda K, Thomas A, et al. A metal-free polymeric photocatalyst for hydrogen production from water under visible light. *Nature Materials*.2009;8:76–80.https://doi.org/10.1038/nmat2317.
15. Thomas A, Fischer A, Goettmann F, et al. Graphitic carbon nitride materials: variation of structure and morphology and their use as metal-free catalysts. *Journal of Materials Chemistry*.2008;18:4893–4908. https://doi.org/10.1039/B800274F.
16. Dong F, Zhao Z, Xiong T, et al. In situ construction of $g-C_3N_4$/$g-C_3N_4$ metal-free heterojunction for enhanced visible-light photocatalysis. *ACS Applied Materials & Interfaces*.2013;5:11392–11401. https://doi.org/10.1021/am402629p.
17. Badger RM. A relation between internuclear distances and bond force constants. *Journal of Chemical Physics*.1934;2:128–131. https://doi.org/10.1063/1.1749396.

18. Zhang J, Zhang M, Zhang G, Wang X. Synthesis of carbon nitride semiconductors in sulfur flux for water photo redox catalysis. *ACS Catalysis*.2012;2:940–948. https://doi.org/10.1021/cs300167d.
19. Ruan, Y.; Hu, Y.; Cheng, H. Recent Progress in g-C_3N_4-Based Photocatalysts for Organic Pollutant Degradation: Strategies to Improve Photocatalytic Activity. *Catalysts* **2025**, *15*, 148. https://doi.org/10.3390/catal15020148.
20. Bhanderi, D.; Patel, M.; Shah, K.; et al. Graphitic Carbon Nitride (g-C_3N_4) as an Emerging Photocatalyst for Sustainable Environmental Applications: A Comprehensive Review. *RSC Sustainability* **2024**, *2*, 1035–1062. https://doi.org/10.1039/D3SU00382E.
21. Bao, T.; Li, X. Recent Advances in the Design and Preparation of Graphitic Carbon Nitride for Photocatalysis. *Chemical Communications* **2025**, *61*, 1509–1523. https://doi.org/10.1039/D4CC04699D.
22. Pantoja-Espinoza, J. C.; DelaCruz-Alderete, G. A.; Paraguay-Delgado, F. Photocatalytic Degradation of Methylene Blue Dye with g-C_3N_4/ZnO Nanocomposite Materials Using Visible Light. *Catalysts* **2025**, *15*, 851. https://doi.org/10.3390/catal15090851.
23. Weldekirstos, H. D. Enhanced Photocatalytic Degradation of Methylene Blue Dye Using g-C_3N_4/$CoFe_2O_4$ Nanocomposite under Sunlight Irradiation. *Journal of Environmental Chemical Engineering* **2024**, *12*, 111234. https://doi.org/10.1016/j.jece.2024.111234.
24. Fang, H.; Wang, J.; Shi, S. Enhanced Visible-Light Photocatalytic Degradation of Methylene Blue via a Ternary Ag_2O@$CuFe_2O_4$@g-C_3N_4 Z-Scheme Heterojunction. *RSC Advances* **2025**, *15*, 39909–39918. https://doi.org/10.1039/D5RA02882E